An experimental study of diffusion and convection of multicomponent gases through catalytic and non-catalytic membranes

Veldsink, J.W.; Versteeg, G.F.; Swaaij, W.P.M. van

Published in:
Journal of Membrane Science

DOI:
10.1016/0376-7388(94)00087-5

ELSEVIER

Journal of Membrane Science 92 (1994) 275–291

journal of MEMBRANE SCIENCE

An experimental study of diffusion and convection of multicomponent gases through catalytic and non-catalytic membranes

J.W. Veldsink*, G.F. Versteeg, W.P.M. van Swaaij

Department of Chemical Engineering, University of Twente, P.O. Box 217, 7500 AE Enschede, Netherlands

(Received January 3, 1994; accepted in revised form March 25, 1994)

Abstract

Diffusion of binary and ternary gases through catalytic and non-catalytic membranes has been studied experimentally at atmospheric pressure. These experiments were conducted in a modified Wicke–Kallenbach diffusion cell consisting of two continuously stirred gas volumes separated by a membrane. The equipment was suitable to measure fluxes of components through the membrane in the absence of gas-to-membrane mass transfer limitations.

Transport through a porous membrane has been measured and compared with the results of the dusty-gas model, which has been used to predict transport through a membrane. With independently determined input parameters this model turned out to be able to predict the transport of a multicomponent gas mixture through a membrane within a few percent ($<5\%$). The Fick model extended with a convective transport contribution was not able to produce similar results as obtained from the dusty-gas model, especially when an overall pressure gradient was present over the membrane.

In order to demonstrate the occurrence of surface effects, dynamic transport of a binary gas was studied in a similar experimental setup as described by Novák et al. In this setup the transport of gas mixtures containing helium, argon and nitrogen was in good agreement with the model simulations. For transport of carbon dioxide and propane through a γ-Al_2O_3 coated membrane, adsorption phenomena were observed, but no substantial surface mobility was detected at temperatures ranging from 293 to 433 K.

Key words: Diffusion and convection; Multicomponent transport; Membrane reactor

1. Introduction

A catalytically active membrane reactor with separated feed of reactants has attractive properties for the processing of fast, heterogeneous gas reactions. Among others, it provides options to improve the reactor control and to avoid the build-up of explosive gas mixtures [2,3]. According to Veldsink et al. [3] slip of unconverted reactants to the opposite side reduces substantially the aforementioned advantages. Therefore, the optimal performance of this type of membrane reactor is obtained for heterogeneous reactions with a high reaction rate compared with the transport rates of reactants through the membrane. Once operated in the de-

*Corresponding author. Present address: Department of Chemical Engineering, University of Groningen, Nijenborgh 4, 9747 AG Groningen, Netherlands.

SSDI 0376-7388(94)00087-F

sired region, transport of components through the membrane becomes the rate governing process. Hence, it is important that a good description of the transport phenomena in the membrane is available and that the transport rate can be estimated accurately.

Transport of components through a porous medium is usually caused by mole fraction gradients as well as total pressure gradients. The transport in the Knudsen regime, with mainly molecule–wall interactions, and in the continuum regime (bulk, molecular regime), where the molecule–molecule interactions are important, is well understood. In the transition region between Knudsen and continuum diffusion an interpolating model (e.g., Bosanquet formula) has to be assumed in order to describe the transport adequately. In addition to the diffusive transport induced by mole fraction gradients, a pressure gradient forces convective motion of the components. To take the effect of both mechanisms into account a more complicated transport model, as for instance the dusty-gas model (DGM), is required to estimate the fluxes through porous media. A detailed theoretical study of transport accompanied with chemical reactions in porous media has already been presented elsewhere [4].

A good description of the transport through (catalytic) membranes is very important for the design of a catalytic membrane reactor and for the interpretation of the experimental data. The transport through porous media has been studied extensively experimentally; most of these studies, however, have either been performed in the Knudsen regime, or dealt with binary mixtures only, because the DGM can be solved explicitly for these systems. Evans et al. [5,6] conducted binary gas diffusion measurements through low-permeability graphite at atmospheric pressure in a Wicke–Kallenbach diffusion cell [1]. The experiments were performed in both the Knudsen and the continuum regime. During these experiments the pressure was kept constant and uniform over the porous solid. Additionally, the effect of an absolute pressure gradient has been studied in the Knudsen regime. Pressure gradient effects in the transition regime were studied by Satterfield and Cadle [7] by using binary mixtures. On transport in multicomponent gases through porous solids less experimental work has been published, which is probably due to the fact that the DGM cannot be solved directly. For transport by diffusion only Remick and Geankoplis [8] solved the DGM equations for a ternary mixture, and presented implicit solutions from which the transport rates, fluxes, can be obtained iteratively. These authors experimentally studied the isobaric diffusion of ternary mixtures (He–Ne–Ar mixtures) through glass capillaries at different absolute pressure levels. By variation of the absolute pressure level the transport process could be studied in the Knudsen regime as well as in the continuum regime. All experiments have been compared to the DGM solutions and showed a good agreement.

Surface mobility of adsorbed species in heterogeneous systems may provide an additional transport mechanism. Surface transport of H_2S and SO_2 in a catalytically active membrane reactor was reported by Sloot et al. [9] for the Claus reaction. The active catalyst for the Claus reaction is γ-Al_2O_3 and its surface OH groups interact with acid gases, such as CO_2 and SO_2. Surface transport of acid gases over γ-Al_2O_3 was also reported by Gilliland et al. [10] and Uhlhorn et al. [11]. These studies showed that the contribution of surface transport is generally small compared with the gas-phase transport. However, because in narrow pores the area of the pore wall is relatively large and the gas-phase transport rate is low, surface diffusion may substantially contribute to the total transport rate. The pore size of the membranes used by Sloot et al. [9], however, were relatively large compared with those used in other studies on surface transport. Yet, they observed a significant contribution of surface transport. The implementation of surface diffusion in the DGM is not as straightforward and simple as compared with pressure and concentration gradient driven transport processes, because no generally accepted description of surface diffusion is available. Basically two approaches have been proposed, a 'hopping' model [10], and a more hydrody-

namic description [12]. A review on the work on surface transport is given by Kapoor et al. [13]. Recently, Krishna [14] developed the crater dusty-gas model, which is a new approach for the description of surface diffusion analogous to the DGM.

As mentioned before, the transport rates completely determine the behaviour of the catalytic membrane reactor with separated feed of reactants. Therefore, the transport of components through a membrane was studied experimentally in the absence of a chemical reaction, and the results are compared with the model calculations on the basis of the DGM. In the present DGM the surface transport was not implemented [4]. First, steady-state diffusion experiments of multicomponent gases (containing, e.g., He, Ar, N_2, CO_2) through a non-catalytic, α-Al_2O_3, membrane are presented, either with or without a pressure difference over the membrane. Owing to its low specific pore area, surface diffusion is not expected to be important in such a membrane. Next, the membrane was wash coated with γ-Al_2O_3 and impregnated with Pt. Provided that no surface transport occurs, the DGM calculations of the steady-state experiments through the impregnated membrane should also be in good agreement with the experimental data.

Additionally, transient diffusion experiments, in which the transport was monitored as a function of time, were carried out in order to study the occurrence of surface effects. Surface transport is usually studied using membranes with narrow pores (high area/volume ratio) and low concentration gradients over the membrane to suppress the gas-phase transport. The surface occupation depends on the composition of the gas phase as expressed by the adsorption isotherm, so that surface transport depends on both the concentration gradient and the actual concentration of a component. Consequently, variation of the gas-phase concentration and simultaneously studying the mole fluxes reveals information on the surface flux. Dynamic diffusion experiments with noble gases were reported by Novák et al. [15] and simulated with a numerically solved transport model. The agreement or mismatching between the experimental and theoretical response curve could possibly give information on surface interactions, such as adsorption and surface mobility.

2. Theory

The transport rate of a component through a membrane is generally determined by three separate steps. First, a species has to be transported from the bulk of the gas phase to the membrane surface, then it is transported through the membrane to the opposite gas–membrane interface followed by transport from this interface to the bulk of the other gas phase. A typical example of a concentration profile over the membrane and its adjacent gas phases is shown in Fig. 1.

The continuity of mass describes the transport through a membrane, and for a flat, one-dimensional geometry this is expressed as:

$$\frac{\epsilon}{RT}\frac{\partial(x_i P)}{\partial t} = -\frac{\partial N_i}{\partial z} \ (\text{mol m}_{\text{cat}}^{-3}\ \text{s}^{-1}) \qquad (1)$$

Two theoretical approaches for the description of transport in porous media have been extensively discussed and it has been concluded that the DGM is preferred for the description of transport through membranes [4]. According to the DGM the transport rate for each component can be calculated from:

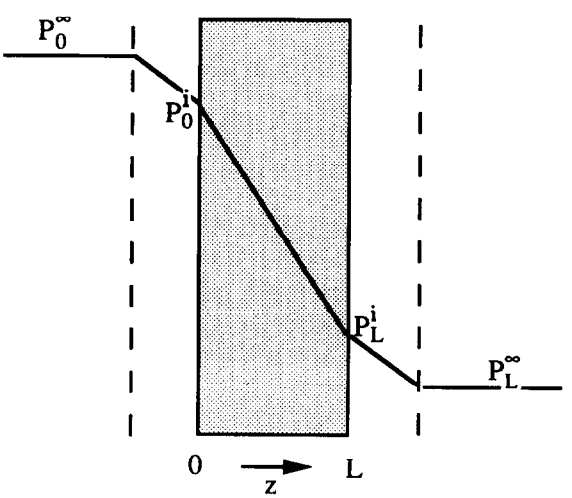

Fig. 1. General partial pressure profile over the membrane and gas phases.

$$\sum_{j=1,j\neq i}^{n}\frac{x_iN_j-x_jN_i}{PD_{ij}^{e}}-\frac{N_i}{PD_{i,K}^{e}}$$
$$=\frac{1}{RT}\cdot\frac{\partial x_i}{\partial z}+\frac{x_i}{PRT}\left(\frac{B_0P}{\mu D_{i,K}^{e}}+1\right)\frac{\partial P}{\partial z}(i=1...n) \quad (2)$$

The diffusion coefficients are effective parameters:

$$D_{i,K}^{e}=\frac{4}{3}K_0\sqrt{\frac{8RT}{\pi M_i}} \quad (m^2\,s^{-1}) \quad (3a)$$

$$D_{ij}^{e}=\frac{\epsilon}{\tau}D_{ij}^{0} \quad (m^2\,s^{-1}) \quad (3b)$$

The structure of the porous membrane is characterized by three parameters, ϵ/τ, K_0 and B_0, which generally have to be determined experimentally from permeation measurements of a single, pure gas through the membrane [16]. For a single gas Eq. (2) reduces to:

$$N_i=\frac{-1}{RT}\left(\frac{B_0P}{\mu}+D_{i,K}^{e}\right)\frac{\partial P}{\partial z} \quad (mol\,m^{-2}\,s^{-1}) \quad (4)$$

Under stationary process conditions the flux is constant and Eq. (4) results in:

$$N_i=\frac{-1}{RT}\left(\frac{B_0(P_L+P_0)}{2\mu}+D_{i,K}^{e}\right)$$
$$\times\frac{(P_L-P_0)}{L} \quad (mol\,m^{-2}\,s^{-1}) \quad (5)$$

According to Eq. (5) the ratio of the flux through the membrane over the pressure difference is proportional to the average pressure. Plotting this ratio as a function of the average pressure, the permeability constant (B_0) results from the slope and the Knudsen constant [K_0, Eq. (3a)] from the intersection with the vertical axis. In the case where the pores are assumed as non-interconnected, circular capillaries of radius r_p, the values of K_0 and B_0 can be calculated directly [16]:

$$K_0=\frac{\epsilon r_p}{2\tau} \quad (m) \quad (6)$$

$$B_0=\frac{\epsilon r_p^2}{8\tau} \quad (m^2) \quad (7)$$

The value of the porosity–tortuosity ratio, ϵ/τ, can be derived from the results of B_0 and K_0:

$$\frac{\epsilon}{\tau}=\frac{K_0^2}{2B_0} \quad (8)$$

However, it is not very likely that in porous membranes the pores are perfectly cylindrical. So, Eq. (8) must be regarded as an approximation, and the porosity–tortuosity ratio also has to be determined experimentally and independently of the other parameters. A well-defined diffusion experiment with a binary gas mixture consisting of noble gases can be used for this purpose.

The overall transport rate of components through a porous matrix (membrane) may not only be determined by the internal resistances, but also gas-to-membrane transfer limitations can become important. Especially in large pore size membranes this external resistance can be significant and the process conditions at the membrane interface may differ substantially from the gas bulk composition. Usually, a gas-phase mass transfer coefficient, k_g, is introduced to describe the external, gas-to-membrane, transport. This coefficient is defined as the ratio of the flux to the membrane and the driving force [17]. Under isothermal conditions,

$$k_g\equiv\frac{RTN_A}{|p_A^{\infty}-p_A^{i}|} \quad (m\,s^{-1}) \quad (9)$$

The value of k_g must be obtained from experiments carried out under well-defined and known bulk and interface conditions. Usually, an evaporating liquid (e.g., *n*-butanol) or a sublimating solid (e.g., naphthalene) is used to provide these conditions. The gas-to-membrane mass transfer coefficient is determined by the hydrodynamics of the system (depending on, e.g., impeller speed and reactor geometry) and physical properties of the gas phase (e.g., viscosity and diffusivity). For a variety of contactors, relations for the calculation of k_g have been reported in the literature, but these are not generally applicable for each specific type of equipment. Therefore, in the present study this parameter was also determined experimentally.

The definition of the gas-to-membrane mass transfer coefficient according to Eq. (9) is restricted to situations with a negligible net molar flux through the interface. If a considerable bulk flow occurs, drag forces will influence the transport process. For processes carried out with porous membranes this situation frequently takes place, for instance by exerting a pressure difference over the membrane. Application of a transmembrane pressure difference results in a convective flow which facilitates the transport of components moving down the pressure gradient and hinders the transport upwards. For this situation [17] the mass transfer coefficient, fluxes, and the gradients are related to one another according to:

$$1+\frac{x_A^0-x_A^\infty}{\frac{N_A}{\sum_{i=1}^{n} N_i}}-x_A^0=\exp\left(\frac{RT\sum_{i=1}^{n} N_i}{Pk_g}\right) \qquad (10)$$

By means of Eqs. (9) and (10) the driving force in a diffusion experiment can be calculated from the observed fluxes and the mass transfer coefficient. In order to compare the calculated fluxes through the membrane with the experimental data, the gas–to–membrane transport resistances must preferably be negligible.

3. Experimental

The steady-state transport of gases (He, Ar, N_2, CO_2, CO, O_2) through the membrane was studied in a modified Wicke–Kallenbach diffusion cell [1]. A flowsheet of the experimental setup is shown in Fig. 2. The cell was constructed of glass, and the two gas volumes (230, 223 ml) were separated by a ceramic membrane of α-Al_2O_3. An oil jacket provided a good temperature control of the cell. Inlet gas flows were preheated by the oil jacket, so that an isothermal operation of the cell was obtained (thermocouple readings within 1°C). Both gas volumes were equipped with a turbine impeller ($d_{imp}=25.10^{-3}$ m; $N_{imp}=0$–30 s^{-1}), and it was assumed that the gas phases were ideally mixed. Gas mixture compositions were set and controlled by Brooks' thermal mass flow controllers. The pressure of each gas volume was controlled by a needle valve present in the outlet. The pressure difference over the membrane was measured by a manometer (mmH_2O reading). In the bottom volume a pressure gauge was installed to read the absolute cell pressure. Effluent gases could be sampled by using a syringe and gas compositions were determined by gas chromatography (Varian 3300) using a Hayesep and a MS5Å column in series. Volumetric outlet gas flows were measured by a soap film flow meter. Finally, the fluxes were calculated from partial mass balances over the gas volumes,

$$0=\Phi_V^{in}\frac{Px_i^{in}}{RT}-\Phi_V^{out}\frac{Px_i^{out}}{RT}-N_iA_m \text{ (mol } s^{-1}) \qquad (11)$$

By imposing the inlet conditions with the mass flow controllers and determining the outlet conditions, the flux can be obtained directly from Eq. (11). The overall fluxes could be measured within a maximum error of 10%.

The gas-to-membrane mass transfer coefficient, k_g, was experimentally determined for the aforementioned diffusion cell from the evaporation rate of *n*-butanol. For this purpose the membrane was removed and the cell was filled with *n*-butanol until the liquid interface was at the same location as the membrane interface. The remaining upper gas volume was continuously fed with pure nitrogen and the *n*-butanol content in the effluent was detected by a thermal conductivity cell. Because the diffusion cell was almost symmetrical it was assumed that the gas-to-membrane mass transfer coefficients in the top and bottom part of the cell are identical.

The dynamic transport experiments were carried out in a modified version of the above-mentioned diffusion cell. One of the gas volumes was replaced by a much smaller volume (4 cm^3), which was closed instead of continuously operated. A digital pressure transducer (Transamerica, 0–0.2 MPa) monitored the pressure in the closed volume. A schematic representation of this modified cell is shown in Fig. 3. The setup closely resembles that of Novák et al. [15], who presented some dynamic diffusion experiments

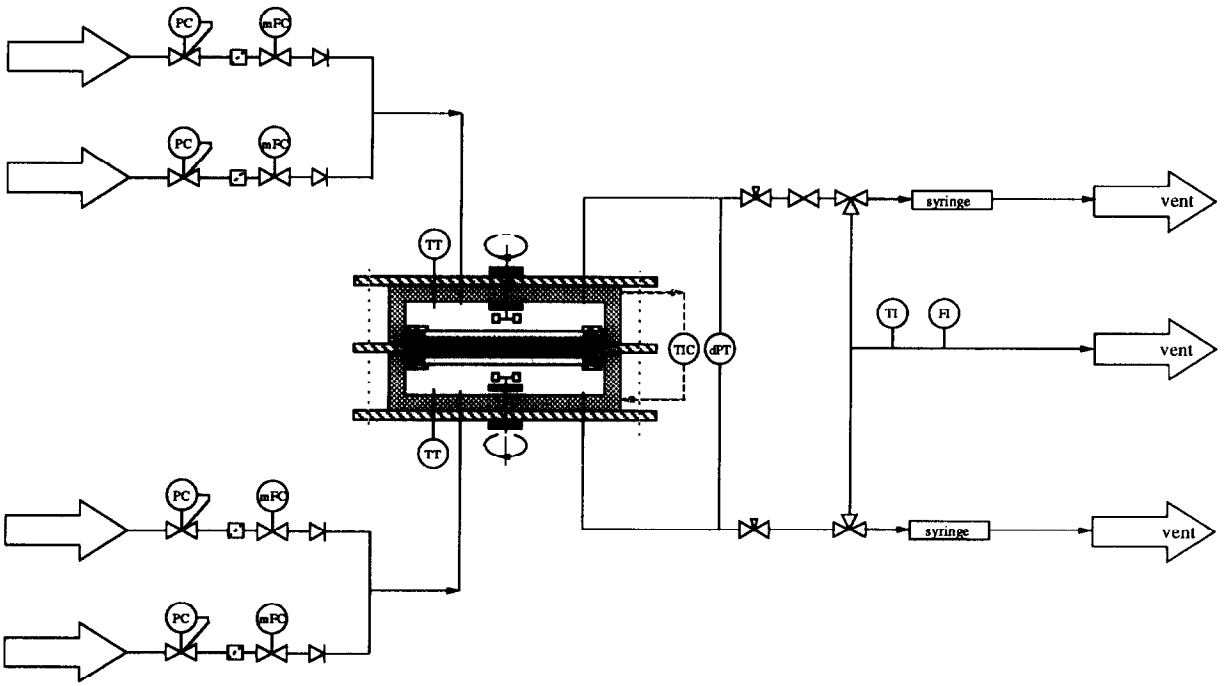

Fig. 2. Flowsheet of the modified Wicke–Kallenbach diffusion cell for steady-state diffusion experiments.

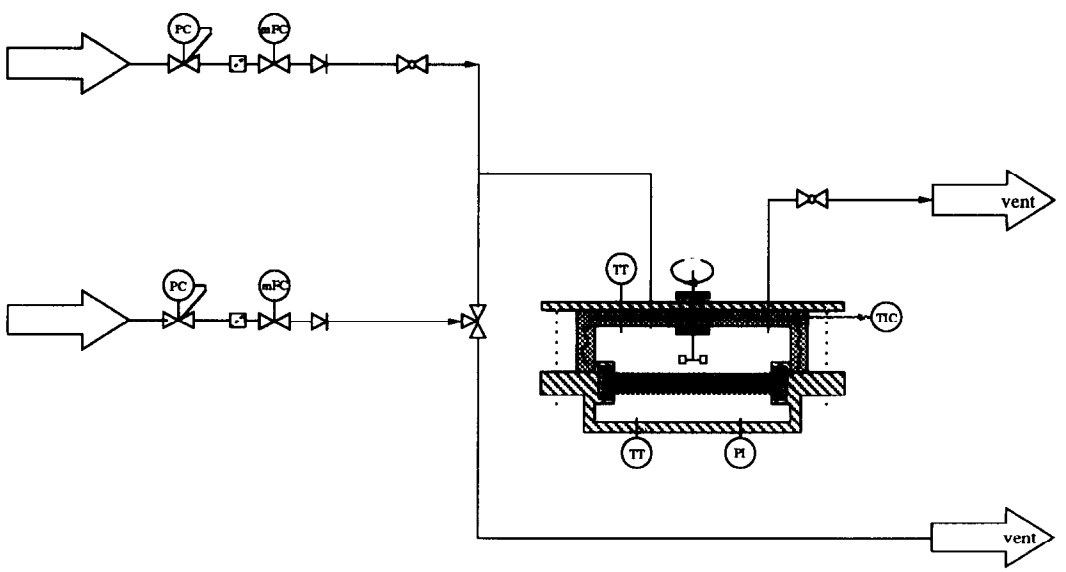

Fig. 3. Flowsheet of the modified diffusion cell for the dynamic diffusion experiments.

through catalyst pellets to verify their dynamic mean-transport-pore model.

4. Results and discussion

Before starting the diffusion experiments on multicomponent gases, it was verified that the transport through the membrane was not limited by gas-to-membrane transport. Therefore, k_g has been measured using the evaporation of *n*-butanol.

To calculate the fluxes through a membrane from the numerical model it is necessary that the values of the structure parameters of the membrane are known. Section 4.2 presents the determination of the structure parameters of the membranes, and, subsequently, flux measurements with both non-catalytic (α-Al_2O_3) and impregnated (Pt/γ-Al_2O_3) membranes.

4.1. Gas-to-membrane mass transfer

The experimental work started with the determination of k_g from the evaporation rate of *n*-butanol. It should be noted that the experimental conditions during these experiments were not similar to those for the transport experiments through the membrane. Especially the hydrodynamics at the gas–liquid and the membrane interface differ substantially. The gas–liquid interface is freely moving, while the interface is fixed for the membranes.

Recently, Kreulen et al. [18] have shown that the gas-phase mass transfer coefficient in gas–liquid stirred cells, similar to the one used in the present study, was not affected by the presence of a polymeric membrane at the interface. As the exact value of k_g is of minor importance for the present study, it is therefore assumed that the values of k_g determined from the butanol evaporation rate can be used for the estimation of the mass transfer coefficients in the experiments with the membranes.

Under the experimental conditions applied in the present study, it turned out that variation of the inlet flow at a constant impeller speed had no effect on the butanol evaporation rate. Hence, the k_g value appeared to be completely determined by the impeller speed. Fig. 4 shows the experimental results at a constant inlet flow rate, which are satisfactorily represented by:

$$k_g = 8.19 \cdot 10^{-4} N_{imp}^{1.2} \ (m\ s^{-1}) \qquad (12)$$

To calculate the mass transfer coefficient for gas mixtures with different physical properties, the results of these experiments were transformed in a dimensionless relation, by using the *Sh*, *Re* and *Sc* numbers on the basis of the impeller geometry. The dependence of the mass transfer coefficient on *Sc* was not investigated in this study, but Versteeg et al. [19] showed that the gas–liquid mass transfer coefficient in a stirred vessel was proportional to $Sc^{0.5}$. Therefore, Eq. (12) was adapted for the estimation of k_g during the membrane experiments according to:

$$\frac{k_g d_{imp}}{D_A^0} = 0.023 \left(\frac{N_{imp} d_{imp}^2 \rho}{\mu} \right)^{1.2} \left(\frac{\mu}{\rho D_A^0} \right)^{0.5} \qquad (12a)$$

or

$$Sh = 0.023 Re_{imp}^{1.2} Sc^{0.5} \qquad (12b)$$

4.2. Determination of the structure parameters

The structure parameters were determined from single gas permeation experiments that were carried out with several gases. Fig. 5 shows a typical result of an experiment performed with he-

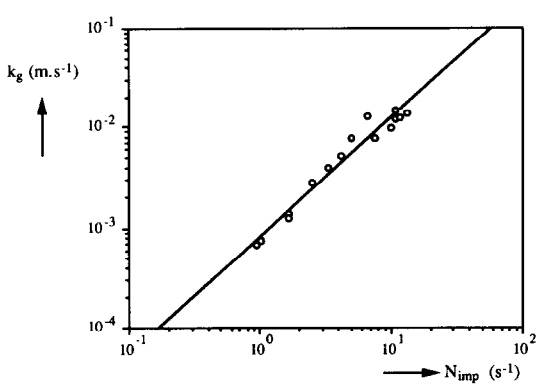

Fig. 4. External mass transfer coefficients obtained from the evaporation rate of *n*-butanol at $T = 293$ K, $P = 0.1$ MPa, and different impeller speed. Physical properties of the gas mixture: $D_{n\text{-}Bu,N_2} = 9.0 \cdot 10^{-6}$ m^2 s^{-1}, $\mu/\rho = 1.52 \cdot 10^{-6}$ m^2 s^{-1}.

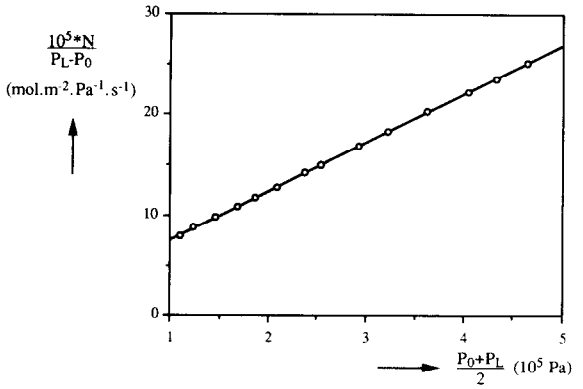

Fig. 5. Permeation of He through the membrane ($L=0.002$ m) at $T=298$ K. The data are plotted in accordance with Eq. (5).

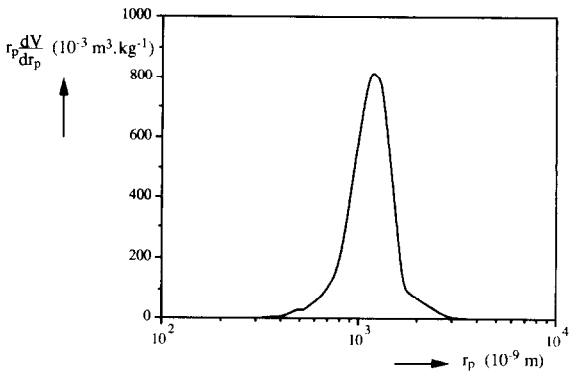

Fig. 6. Pore-size distribution of a membrane resulting from mercury porosimetry.

Table 1
Structure parameters of the membrane resulting from permeation measurements with gases

gas	B_0 $\times 10^{-14}$ (m^2)	K_0 $\times 10^{-7}$ (m)	r_p $\times 10^{-6}$ (m)
N_2	4.74	1.14	1.66
	4.83	1.06	1.82
He	5.02	0.97	2.07
Ar	4.85	1.06	1.83

lium presented graphically in accordance with Eq. (5). Table 1 presents the results obtained from other gases. Within the experimental accuracy, the values of the parameters are independent of the gas.

From the structure parameters that were obtained, the pore radius was calculated assuming that the pores are ideally cylindrical, i.e.:

$$r_p = \frac{4B_0}{K_0} \tag{13}$$

Fig. 6 shows the corresponding mercury porosigram of the membrane, and it can be seen that a narrow, unimodal pore size distribution is present with an average pore radius of $r_p = 1.2$ μm. The pore radii calculated from Eq. (13) with the structure parameters given in Table 1 are close to this value, but nevertheless systematically higher. This is explained by the fact that the permeability factor, B_0, is proportional to the average of the square of the pore radii, whereas the Knudsen constant, K_0, is proportional to the average of the pore radii, respectively. It can thus be shown that, for any pore size distribution, Eq. (13) overestimates the average pore radius.

Finally, the porosity–tortuosity ratio was obtained from the best fit of an isobaric binary diffusion experiment of nitrogen and helium at ambient pressure and temperature. This resulted in a value of $\epsilon/\tau = 0.147$, which is in good agreement with the value calculated from Eq. (8), $\epsilon/\tau = 0.126$. Consequently, the experimentally determined structure parameters of the membrane are: $B_0 = 4.79 \cdot 10^{-14}$ (m^2), $K_0 = 1.10 \cdot 10^{-7}$ (m), and $\epsilon/\tau = 0.147$. With these values and known gas compositions at the membrane interfaces, the fluxes can be calculated from Eqs. (1) and (2).

During the determination of the porosity–tortuosity ratio from an isobaric flux measurement of a He–N_2 mixture, it turned out that a gas-to-membrane transport resistance (10%) had to be taken into account. This influence of the external resistance could be reduced by increasing the transport resistance through the membranes, by placing several membranes in series. For two membranes in series the total gas-to-membrane mass transfer resistance is already less than 5% compared with the total membrane resistance. Therefore, all experiments were conducted with two membranes in series.

4.3. Diffusion of N_2–Ar–He through a membrane.

First diffusion experiments of He–Ar–N_2 mixtures were carried out in the diffusion cell at atmospheric pressure and ambient temperature. An α-Al_2O_3 membrane which was not impregnated with any catalytic material was present in the diffusion cell. Hence, surface effects were not expected in these experiments and the model predictions of the fluxes should be in good agreement with the experimental data. In the calculations the gas-to-membrane transport resistance was neglected (<3%).

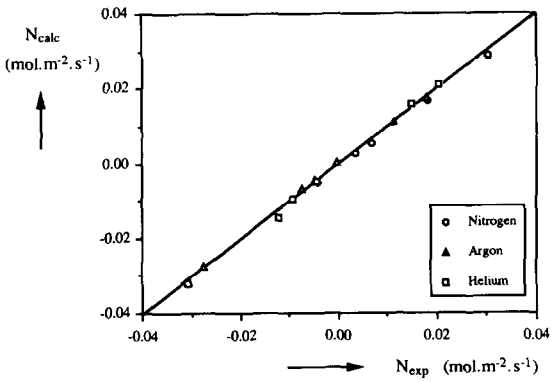

Fig. 7. Diffusion of He–Ar–N_2 through a porous membrane at P=0.12 MPa and T=298 K. Parity plot of the calculated flux from the dusty-gas model, Eq. (2), and the experimental flux.

Table 2
Experimental conditions for diffusion experiments of He, Ar and N_2 mixtures through a membrane at T=298 K

No.	P_L (MPa)	P_0-P_L (mmHg)	$x_{N_2,0}$	$x_{N_2,L}$	$x_{Ar,0}$	$x_{Ar,L}$
1	0.12	93	0.2862	0.4082	0.1975	0.5951
2		−119	0.6202	0.1798	0.5212	0.1190
3		23	0.6657	0.1503	0.3640	0.3507
4		80	0.6871	0.1341	0.3395	0.3805
5	0.20	3	0.7211	0.1056	0.4485	0.2261
6		80	0.8225	0.1762	0.5126	0.1331
7		−73	0.6212	0.0432	0.3575	0.3590
8	0.30	−45	0.6302	0.1685	0.5028	0.1481
9		7	0.7331	0.0969	0.4330	0.2493
10		31	0.7725	0.0714	0.3993	0.2975

Table 3
Comparison of experimental fluxes with the calculations according to different models[a]

No.[b]		N_{N_2}	N_{Ar}	N_{He}
		10^{-3} (mol m^{-2} s^{-1})		
1	exp.	3.441	17.93	20.40
	DGM	2.481	17.55	20.70
	lin. DGM	2.387	16.16	19.82
	Fick	−2.089	15.43	16.41
2	exp.	6.783	−27.60	−30.70
	DGM	5.243	−27.58	−32.17
	lin.DGM	4.091	−24.83	−30.68
	Fick	9.087	−24.84	−25.32
3	exp.	18.25	−4.728	−9.381
	DGM	16.88	−4.401	−9.673
	lin.DGM	16.20	−4.400	−9.640
	Fick	16.50	−6.183	−8.842
4	exp.	30.55	−0.201	−4.464
	DGM	28.60	0.281	−4.698
	lin.DGM	26.81	0.413	−4.971
	Fick	24.65	−2.306	−5.300
5	exp.	22.90	−11.80	−18.70
	DGM	20.53	−10.33	−17.66
6	exp.	8.052	−26.76	−30.44
	DGM	5.516	−26.08	−30.39
7	exp.	53.76	−2.711	−7.917
	DGM	50.79	−1.825	−6.970
8	exp.	9.852	−24.80	−29.10
	DGM	6.455	−23.78	−28.40
9	exp.	26.91	−10.30	−17.20
	DGM	22.24	−9.209	−16.26
10	exp.	33.74	−6.424	−13.05
	DGM	33.06	−5.113	−11.66

[a]Model parameters in the calculations: $B_0=4.79\cdot10^{-14}$ m^2; $K_0=1.10\cdot10^{-7}$ m; $\epsilon/\tau=0.147$; $D_{N_2,Ar}=1.95\cdot10^{-5}$, $D_{N_2,He}=7.072\cdot10^{-5}$, $D_{He,Ar}=7.355\cdot10^{-5}$ m^2 s^{-1}; $m=2.011\cdot10^{-5}$ Pa s.
[b]Numbers correspond to the conditions presented in Table 2.

Flux measurements at 0.12 (MPa) and 298 (K) are presented in Fig. 7 as a parity plot between the experimentally observed fluxes and the

model predictions. A good agreement exists as can be concluded from this diagram. Table 2 summarizes the experimental conditions for ten typical experiments. The measured fluxes corresponding to these experiments are presented in Table 3 together with the model calculations. Although during the experiments the pressure differences over the membrane were small in comparison with the absolute pressure level, convective flows equal to the diffusion fluxes were induced because of the relatively large pore diameters of the membrane.

The left column of Table 3 also shows the fluxes calculated from an approximation of the DGM as proposed by Krishna [20] as well as the Fick model extended with a convective flow contribution (see ref. 4). Apparently, the best agreement is obtained by the complete DGM, although the linearized DGM also shows a remarkable agreement. This approximate model assumes straight mole fraction profiles a priori, so that the fluxes can be calculated directly from the equations. The results are satisfactorily accurate, even under conditions with a substantial convective flow. This is noteworthy because for the latter situation the profiles are usually curved, owing to the presence of a pressure gradient and the linearization, therefore, seems questionable. For two cases presented, the results of the Fick model largely differ from the DGM results. In experiment No. 1 nitrogen is transported through the membrane against its gradient, caused by a convective flow. The Fick model calculates the diffusion flux of a particular component directly from its partial pressure gradient and adds the viscous flow to the diffusion flux [4]. For this situation it predicts a net nitrogen flux that is in the opposite direction. A similar situation occurred in experiment No. 4 for the argon flux. In this experiment the diffusion flux of argon is nearly balanced by an opposing convective motion, so that its net flux is close to zero. Although the direction of the argon transport is correct, the Fick model calculates a ten times higher flux. The deviation of the DGM can be attributed to the fact that the external mass transfer was not taken into account in the calculations.

From the He–Ar–N_2 diffusion experiments, it is concluded that the DGM accurately predicts the fluxes through the membrane without any adjustable parameters. The simplified procedure suggested by Krishna [20] also performs well, even when a viscous flow is present and the profiles are no longer linear due to the presence of a pressure gradient. The coupling of the diffusion fluxes (drag effects) seems to be more important than the use of the exact, local values of the gradients inside the membrane. Therefore, the extended Fick model, which neglects these coupling effects, results sometimes not only in quantitative errors, but also in large qualitative deviations. This is all in line with the conclusions from a detailed comparison of the DGM and the Fick model [4].

4.4. Transport through a catalytically active membrane

Once it was verified that the diffusion process in the diffusion cell was well described by the DGM, the α-Al_2O_3 membranes were impregnated with catalytic material, Pt/γ-Al_2O_3. First, a γ-Al_2O_3 wash coat was deposited on the pore walls by absorbing an aqueous solution of urea and aluminium nitrate (mass ratio 1:2) in the pores. Then the membrane was heated up quickly to 373 K and dried at this temperature for one night. Subsequently, the nitrous compounds were

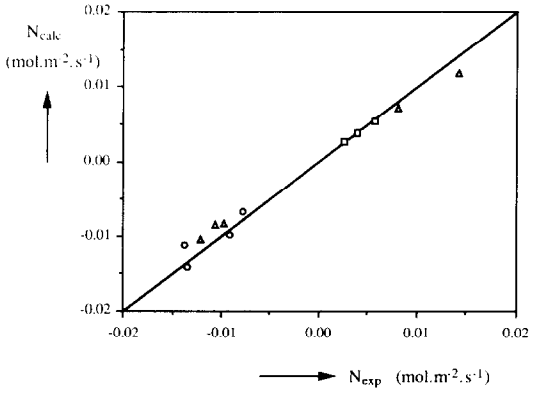

Fig. 8. Parity plot of the calculated (DGM) and experimental flux of CO (△), O_2 (□), and CO_2 (○) through the membrane impregnated with Pt/γ-Al_2O_3. Table 4 shows the experimental conditions.

Table 4
Experimental conditions of the flux measurements through an alumina membrane impregnated with Pt/γ-Al_2O_3[a]

No.	P_L (MPa)	T (K)	P_0-P_L (mmH_2O)	$x_{1,0}$	$x_{1,L}$	$x_{2,0}$	$x_{2,L}$
$x_1=N_2, x_2=CO_2$							
1	0.12	298	−1	0.8707	0.2056	0.1293	0.7944
2			48	0.9133	0.2706	0.0867	0.7294
3		333	−4	0.8679	0.2099	0.1321	0.7901
4			48	0.9022	0.2658	0.0978	0.7342
$x_1=Ar, x_2=N_2, x_{CO}=1-x_1-x_2$							
5	0.20	298	0	0.1277	0.7065	0.4454	0.1515
6			−14	0.7130	0.1217	0.1461	0.4505
7		396	65	0.0952	0.5873	0.4607	0.2081
8			−6	0.6884	0.1490	0.1568	0.4337
9			−39	0.6567	0.1276	0.1728	0.4431
$x_1=He, x_2=N_2, x_{O_2}=1-x_1-x_2$							
10	0.12	397	59	0.2399	0.5095	0.6008	0.3869
11			130	0.2162	0.4785	0.6196	0.4120
12			−4	0.2610	0.5355	0.5842	0.3665

[a]Structure parameters of the membrane: $B_0=3.019\cdot10^{-14}$ m^2, $K_0=9.22\cdot10^{-8}$ m, $\epsilon/\tau=0.115$.

removed from the surface at 473 K and afterwards the membrane was calcined for 4 h at 673 K. Secondly, the membrane was impregnated with platinum by using an aqueous H_2PtCl_6 solution. The impregnated membranes contained ~6.5 wt% γ-Al_2O_3 and 3.0 wt% Pt. Transport of components occurring in oxidation reactions (e.g., CO, CO_2, O_2) through this catalytically active membrane was studied at low temperatures ($T<423$ K).

Fig. 8 summarizes a number of experiments, showing a parity plot between the calculated flux and the experimentally observed flux of some components. The experimental conditions are presented in Table 4. From Fig. 8 it is concluded that all fluxes are accurately predicted by the DGM. The fluxes of nitrogen are not shown in Fig. 8, but were also accurately predicted as was demonstrated in previous experiments. From the results of Fig. 8 and similar experiments, it was concluded that additional transport due to surface interactions of CO2, CO, CH_4, O_2, and N_2 did not occur at temperatures between 298 and 400 K and pressures between 0.1 and 0.3 MPa.

4.5. Dynamic transport of a binary gas mixture

From the steady-state measurements it can be concluded that no surface diffusion was detected in an α-Al_2O_3 membrane impregnated with γ-Al_2O_3 and Pt and an average pore size of 1 μm. In large pores the gas-phase transport is favoured due to the fact that the surface transport coefficients are usually much smaller [21]. Therefore additional experiments were carried out using a smaller pore-size membrane in order to investigate the possible occurrence of surface diffusion. However, the diffusion process remained in the transition regime. A membrane with an average pore size of $d_p\approx0.1$ μm was impregnated with γ-Al_2O_3 (1.9 wt%, calcined at 450°C) to create sites for acid–base interactions between the gas and the surface. Especially carbon dioxide is expected to be influenced by the presence of surface OH groups. The structure parameters for this membrane are presented in Table 5, and were determined as discussed in the previous sections. Surface transport depends not only on the concentration gradient, but also on the absolute concentration level. Therefore, the diffusion process is monitored as a function of time after

Table 5
Structure parameters of the membrane used in the transient experiments together with the binary diffusion coefficient at atmospheric pressure

Structure parameters	Diffusion coefficients ($m^2 s^{-1}$)	T (K)
$K_0 = 3.24 \cdot 10^{-9}$ m	$D^0_{He,Ar} = 7.34 \cdot 10^{-5}$	293
$B_0 = 5.89 \cdot 10^{-17}$ m^2	$D^0_{He,Ar} = 13.250 \cdot 10^{-5}$	415
$\epsilon/\tau = 0.080$	$D^0_{He,N_2} = 7.168 \cdot 10^{-5}$	298
$r_p = 4.44 \cdot 10^{-8}$ m	$D^0_{He,CO_2} = 5.792 \cdot 10^{-5}$	293
(mercury porosimetry)	$D^0_{He,CO_2} = 11.384 \cdot 10^{-5}$	434
	$D^0_{He,Prop} = 4.158 \cdot 10^{-5}$	298
	$D^0_{He,Prop} = 7.336 \cdot 10^{-5}$	416

a step change was imposed on the inlet conditions.

To perform dynamic transport experiments the original experimental setup was modified as described in section 3 and is shown in Fig. 3. During the dynamic diffusion experiments the (absolute) pressure in the closed gas volume was monitored as a function of time. As indicated by Novák et al. [15] the pressure should increase in the closed-volume part of the setup when a heavy gas, present in this volume, is exchanged for a lighter component because the latter is transported faster through the membrane. According to Graham's law of diffusion,

$$\sum_{i=1}^{n} N_i \sqrt{M_i} = 0 \tag{14}$$

in the case where the diffusion process is either isobaric or in the Knudsen regime. Initially, the system is isobaric and the transport rates through the membrane are related to the square root of the molecular mass, resulting in non-equimolar flows when the molar masses are different. A total mass balance over the closed volume reads

$$\frac{V}{RT} \cdot \frac{\partial P}{\partial t} = -A_m \sum_{i=1}^{n} N_i(z=0) \tag{15}$$

Owing to the non-equimolar flow, the right-hand side of Eq. (15) is not equal to zero and causes a change in the cell pressure. The magnitude of the pressure effects are determined by the difference in molecular mass of the components, the size of the closed volume and the membrane structure parameters. If the pressure changes, the viscous flow will induce transport in the opposite direction, and the pressure gradient over the membrane gradually returns back to zero.

From the previous sections, it was already concluded that the steady-state transport fluxes through the membrane were correctly described by the DGM without any adjustable parameters and surface transport. As a check on the ability to predict also the time-dependent transport through a membrane, the diffusion of noble gases (He–Ar) through the membrane was studied first. For noble gases surface effects are not expected. In order to realise a reasonable pressure change the volume of the modified cell was kept as small as possible, and, therefore, the impeller was removed from the closed volume. The removal of the impeller, however, might introduce a gas-to-membrane mass transfer resistance, since the gas phase is completely stagnant. The presence of external mass transport limitations in the closed volume was estimated from $Sh = 2.47$, which has been derived from the penetration theory [17]. From this value of Sh, gas-to-membrane transport limitations turned out to be negligible ($< 4\%$).

Initially, the cell was filled with Ar and, at $t = t_0$, He was continuously supplied to the upper part of the cell at such a high flow rate that almost instantaneously ($t < 1$ s) the contents of this volume was replaced by He, invoking a step change in the composition. Now the diffusion process forces the cell to a new steady state corresponding to the newly imposed process conditions. Since He moves more rapidly through the membrane than Ar, the pressure in the closed volume increases. The experimental pressure and the model prediction are presented as a function of time in Fig. 9. Fig. 9 also shows the reverse case, exchanging He by Ar, and both cases show a good agreement of the model calculations with the experimental data. Furthermore, different symbols for both types of experiment illustrate a good reproducibility of these experiments. Fig. 10 demonstrates that a good agreement is also observed at higher temperatures.

The model simulations were carried out with-

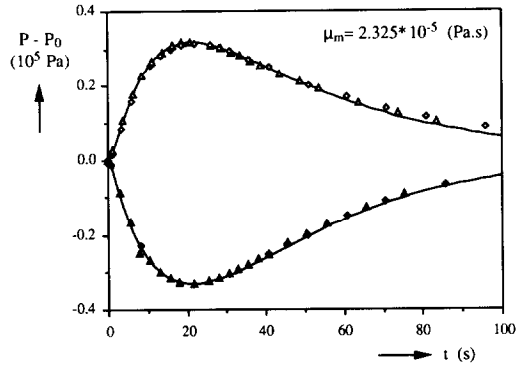

Fig. 9. Transient diffusion experiment of He and Ar at $T=293$ K. The open symbols show the pressure–time readings when the cell was initially filled with Ar, whereas the closed symbols represent the data when the cell was initially filled with He. The lines are the predictions according to the dusty-gas model.

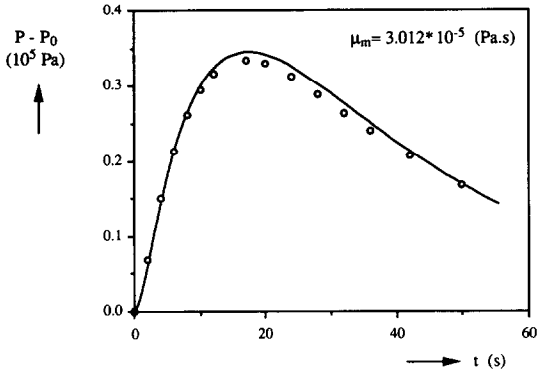

Fig. 10. Transient diffusion experiment of He–Ar system at $T=415$ K. Comparison of experiment with dusty-gas model.

out the use of any adjustable parameters. The structure parameters were determined in separate and independent experiments. The binary diffusion coefficients were obtained from Marrero and Mason [22], and the viscosity of the pure components were obtained from Landolt-Börnstein [23] as a function of temperature. In the model a mixture viscosity was used, calculated according to the Wilke mixture rule [24], and kept constant during the calculations. The mixture viscosity was evaluated at a mixture composition of 50% of both components and the value is given in the different diagrams.

Secondly, the dynamic diffusion of a He–N_2 system was studied at 298 K. For this system also no important surface interactions are to be expected. The results are shown in Fig. 11 and it was observed that the results were in good agreement again. From Figs. 9–11 it can be concluded that the model is able to predict the dynamic transport through a membrane without the implementation of a surface diffusion contribution.

Finally, two systems were studied which are expected to show surface interactions. From Ulhorn et al. [11] a small surface contribution could be expected for CO_2 and hydrocarbons. The CO_2 adsorption on γ-Al_2O_3 was well studied [25]. At low temperatures CO_2 is adsorbed as a relatively immobile bicarbonate complex, but at elevated temperatures the adsorbed species changes into a super mobile carbonate complex. Rosynek [25] reports on his catalyst a transition temperature of 423 K. Therefore, transport of CO_2 through the membrane was studied at low (293 K) and elevated (434 K) temperatures, and the results are presented in Fig. 12 and 13. Contrary to the previous results on the He–Ar and He–N_2 systems a significant discrepancy is observed between the experimental data and the model calculations. These deviations can be attributed to surface interactions. From the steady-state transport experiments presented in the previous section, it was concluded that surface interactions were not noticed and the fluxes of CO_2 were accurately described by the model.

From Fig. 12 it can be concluded that the largest discrepancies are observed in the case where

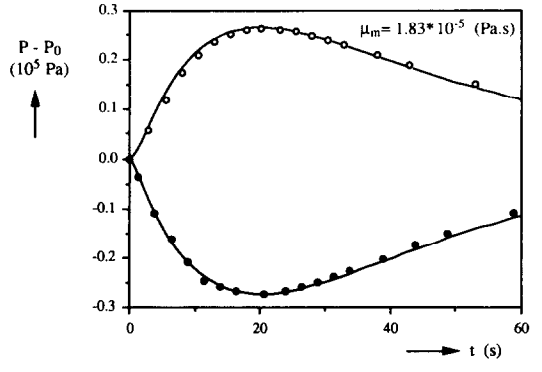

Fig. 11. Transient diffusion experiment of He–N_2 system at $T=298$ K. Comparison of experiment with dusty-gas model.

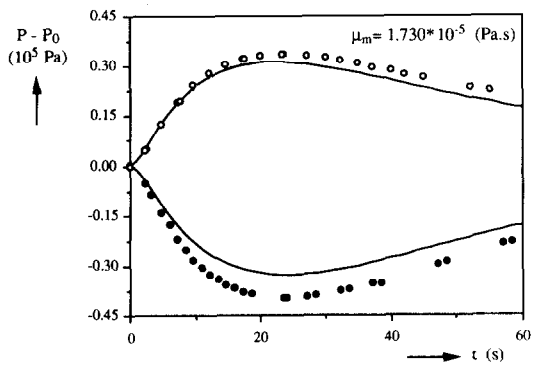

Fig. 12. Transient diffusion experiment of He–CO_2 system at $T=293$ K. Comparison of experiment with dusty-gas model.

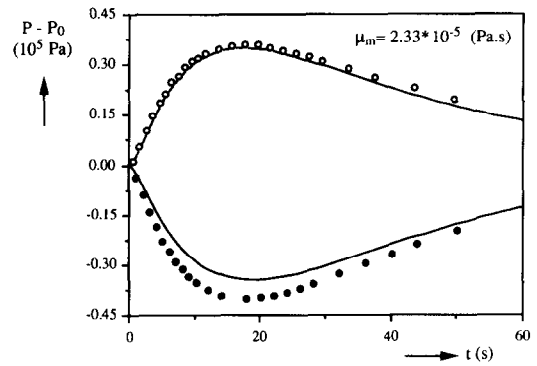

Fig. 13. Transient diffusion experiment of He–CO_2 system at $T=434$ K. Comparison of experiment with dusty-gas model.

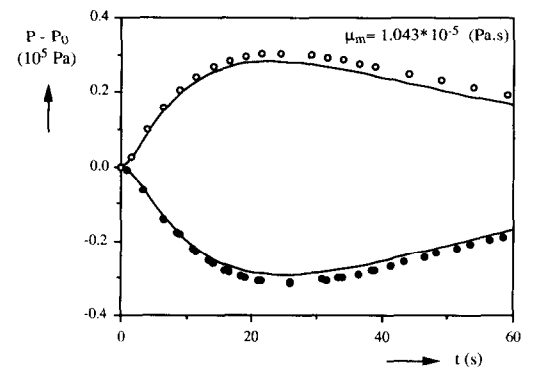

Fig. 14. Transient diffusion experiment of He–C_3H_8 system at $T=298$ K. Comparison of experiment with dusty-gas model.

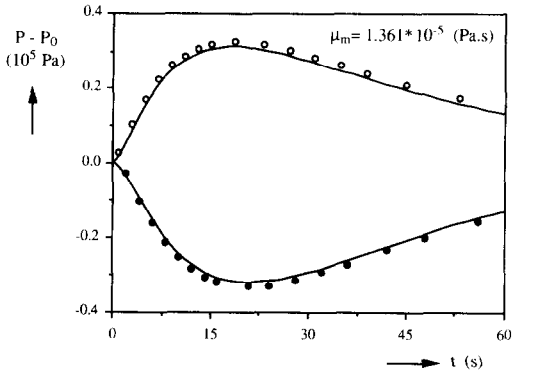

Fig. 15. Transient diffusion experiment of He–C_3H_8 system at $T=416$ K. Comparison of experiment with dusty-gas model.

the pores are initially filled with He and subsequently replaced by CO_2 (negative response curve). In this case the surface is initially free from CO_2 and instead of being transported through the pores to the opposite side CO_2 adsorbs on the pore wall, whereas He moves unaffectedly through the membrane. So, the He outflux of the closed volume is compensated by a much smaller influx of CO_2, which results in a larger pressure decrease than calculated from the model. According to the adsorption isotherm, at higher temperatures less CO_2 adsorbs, so that the discrepancy between the model and the experimental data becomes smaller. This is shown in Fig. 13.

Figs. 12 and 13 also show that the He–CO_2 (negative) and CO_2–He (positive) curves are not symmetrical, and that the CO_2–He curve shows a better agreement with the model calculations. In this case the pores are initially filled with CO_2, so that the surface is completely occupied with CO_2. Instead of adsorption, now desorption occurs. According to Rosynek [25] the desorption rate is very low which explains the better agreement of the CO_2–He curve with the calculations. Therefore, initially the gas-phase transport rate is not influenced by this phenomenon, and the experiments and model simulations are in good agreement. Next, the desorption process starts to affect the gas-phase profile of CO_2 and owing to this effect its concentration gradient decreases. Therefore, less CO_2 is trans-

ported through the membrane than expected, causing a pressure increase in the closed volume. At higher temperatures the CO_2 occupation on the surface is lower resulting in smaller deviations (see Fig. 13). Additional experiments were carried out at different temperatures, $293 \leqslant T \leqslant 434$ K, which showed similarly shaped pressure–time trajectories. Therefore, it is not likely that the surface mobility has changed significantly over this temperature range. Due to temperature limitations, the supermobile carbonate surface species could not be observed in the present experimental equipment and for the present catalyst.

Finally, dynamic transport of propane through the membrane was studied and the results are presented in Fig. 14 and 15. Contrary to carbon dioxide, alkanes show higher desorption rates [26] and now the experimental curves are almost symmetrical. At higher temperatures a good agreement is observed, owing to less adsorption.

5. Conclusions

A steady-state diffusion cell was constructed to study the transport of components through a membrane. The gas-to-membrane transport limitations could be neglected under the experimental conditions used in the present study. Diffusion experiments of several gases through catalytically active and non-active membranes were carried out, and the transport rates were compared with the dusty-gas model (DGM) calculations. With independently determined structure parameters it was shown that the DGM is able to predict the transport through membranes with high accuracy. Calculations according to the Fick model were also compared with the experimental results and, occasionally, this model shows large deviations with the experimental results or the DGM calculations. For steady-state calculations the approximated DGM as suggested by Krishna [20] estimates satisfactorily the transport rates, even in the presence of a substantial viscous flow. This approximated model does not require elaborate mathematical techniques and is therefore recommended for the calculation of steady-state fluxes.

In order to study surface effects during the transport of components, a dynamic diffusion cell was used similar to the apparatus of Novák et al. [15]. In the absence of surface interactions, dynamic, non-isobaric diffusion through a membrane is well described by the DGM. To study the influence of adsorption and desorption processes of components, a dynamic diffusion experiment may yield useful information concerning the mobility of the components. For CO_2 and propane, transport through the membrane was affected by adsorption. The hysteresis between the adsorption and desorption isotherm is revealed by the asymmetry of the experimental response curves. Surface mobility of CO_2 could not be detected because of the limited temperature range of the experimental setup. Nevertheless, the dynamic diffusion cell seems a promising technique for studying surface effects on the transport of components through porous materials.

6. List of symbols

A_m	external membrane area (m^2)
B_0	d'Arcy permeation constant (m^2)
d	diameter or characteristic length in Sh (m)
D_{ij}	binary diffusion coefficient between i and j ($m^2\ s^{-1}$)
$D_{i,K}$	Knudsen diffusion coefficient of component i ($m^2\ s^{-1}$)
k_g	gas-to-membrane mass transfer coefficient ($m\ s^{-1}$)
K_0	Knudsen constant (m)
M	molecular mass ($kg\ .mol^{-1}$)
N	molar flux ($mol\ m^{-2}\ s^{-1}$)
N_{imp}	rotational speed of impeller (s^{-1})
P	pressure (Pa)
p_i	partial pressure of component i (Pa or mmH_2O)
R	universal gas constant ($J\ mol^{-1}\ K^{-1}$)
Re_{imp}	Reynolds number, based on the rotational speed of the impeller, $N_{imp}d_{imp}^2\rho/\mu$

r	radius (m)
Sc	Schmidt number, $\mu/\rho D^0_A$ (–)
Sh	Sherwood number, $k_g d_{imp}/D^0{}_A$ (–)
t	time (s)
T	temperature (K)
V	volume (m^3)
x	mole fraction (–)
z	space co-ordinate (m)
ϵ	porosity (–)
τ	tortuosity (–)
μ	viscosity (Pa s)
ρ	density ($kg\ m^{-3}$)
Φ_v	volumetric flow rate ($m^3\ s^{-1}$)

6.1. Subscripts/superscripts

A,*i*,*j*	with respect to component A, *i* or *j*, respectively
e	effective
in	inlet
m	mixture
out	outlet
imp	impeller
p	pore
0,*L*	at the beginning and end of the membrane, respectively
0	gas-phase conditions
i	interface (membrane–gas)
∞	gas bulk

Acknowledgements

These investigations were not possible without the financial support of GASTEC, Apeldoorn, Netherlands. For their help in the experimental work we greatfully acknowledge the contributions of G.H.W. van Benthem and A. van Waveren. For his technical assistance we appreciate the work of A. Schanssema. Thanks also to M. Bracht for his work on the development of the computer program.

References

[1] E. Wicke and R. Kallenbach, Die Oberflächendiffusion von Kohlendioxyd in aktiven Kohlen, Kolloid Z., 97 (1941) 135–151.

[2] H.J. Sloot, G.F. Versteeg, W.P.M. van Swaaij, A non-permselective membrane reactor for chemical processes normally requiring strict stoichiometric feed rates of reactants, Chem. Eng. Sci., 45 (1990) 2415–2421.

[3] J.W. Veldsink, R.M.J. van Damme, G.F. Versteeg and W.P.M. van Swaaij, A catalytically active membrane reactor for fast, exothermic, heterogeneously catalysed reactions, Chem. Eng. Sci., 47 (1992) 2939–2944.

[4] J.W. Veldsink, A Catalytically Active, Non-permselective Membrane Reactor for Kinetically Fast, Strongly Exothermic, Heterogeneous Reactions, Thesis, University of Twente, Enschede, Netherlands, 1993.

[5] R.B. Evans, G.M. Watson and J. Truit, Interdiffusion of gases in low-permeability graphite at uniform pressure, J. Appl. Phys., 33 (1962) 2682–2688.

[6] R.B. Evans, G.M. Watson and J. Truit, Interdiffusion of gases in low-permeability graphite. II. Influence of pressure gradients, J. Appl. Phys., 34 (1963) 2020–2026.

[7] C.N. Satterfield and P.J. Cadle, Gaseous diffusion and flow in commercial catalysts at pressure levels above atmospheric, Ind. Eng. Chem. Fundam., 7 (1968) 202–210.

[8] R.R. Remick and C.J. Geankoplis, Ternary diffusion of gases in capillaries in the transition region between Knudsen and molecular diffusion, Chem. Eng. Sci., 29 (1974) 1447–1455.

[9] H.J. Sloot, C.A. Smolders, W.P.M. van Swaaij and G.F. Versteeg, Surface diffusion of hydrogen sulfide and sulfur dioxide in alumina membranes in the continuum regime, J. Membrane Sci., 74 (1992) 263–278.

[10] E.R. Gilliland, R.F. Baddour, G.P. Perkinson and K.J. Sladek, Diffusion on surfaces. I. Effect of concentration on the diffusivity of physically adsorbed species, Ind. Eng. Chem. Fundam., 13 (1974) 95–105.

[11] R.J.R. Uhlhorn, K. Keizer and A.J. Burggraaf, Gas and surface diffusion in modified γ-alumina systems, J. Membrane Sci., 46 (1989) 225–241.

[12] M. Asaeda, J. Watanabe, Y. Matono, K. Kojima and R. Toei, Combined surface and gas phase diffusion through plugs of porous adsorbent in transition diffusion region, Chem. Eng. Jpn., 14 (1981) 13–19.

[13] A. Kapoor, R.T. Yang and C. Wong, Surface diffusion, Catal. Rev.-Sci. Eng., 31 (1989) 129–214.

[14] R. Krishna, Problems and pittfalls in the use of the Fick formulation for intraparticle diffusion, Chem. Eng. Sci., 48 (1993) 845–861.

[15] M. Novák, K. Ehrhardt, K. Klusácek and P. Schneider, Dynamics of non-isobaric diffusion in porous catalysts, Chem. Eng. Sci., 43 (1988) 185–193.

[16] E.A. Mason and A.P. Malinauskas, Gas Transport in Porous Media: The Dusty Gas Model, Elsevier, Amsterdam, 1983.

[17] R.B. Bird, W.E. Stewart and E.N. Lightfoot, Transport Phenomena, Wiley, New York, 1960.

[18] H. Kreulen, C.A. Smolders, G.F. Versteeg and W.P.M. van Swaaij, Determination of mass transfer rates in wetted and non-wetted microporous membranes, Chem. Eng. Sci., 48 (1993) 2093–2102.

[19] G.F. Versteeg, P.M.M. Blauwhoff and W.P.M. van Swaaij, The effect of diffusivity on gas–liquid mass transfer in stirred vessels, Chem. Eng. Sci., 42 (1987) 1103–1119.

[20] R. Krishna, A simplified procedure for the solution of the dusty gas model equations for steady-state transport in non-reacting systems, Chem. Eng. J., 35 (1987) 75–81.

[21] T.T. Tsotsis, R.C. Sane, I.A. Webster and J.D. Goddard, Theoretical and experimental aspects of surface diffusion in porous catalysts. I. Non-reactive conditions, J. Catal., 101 (1986) 416–427.

[22] T.R. Marrero and E.A. Mason, Gaseous diffusion coefficients, J. Phys. Ref. Data, 1 (1972) 3–118.

[23] K. Schäfer (Ed.), Landolt-Börnstein, Zahlenwerte und Funktionen aus Physik, Chemie, Astronomie, Geophysik und Technik, Band II, Teil 5a, Transportphänomenen I, Springer Verlag, Berlin, 1969.

[24] R.C. Reid, J.M. Prausnitz and B.E. Poling, Properties of Gases and Liquids, 4th ed., McGraw-Hill, New York, 1987.

[25] M.P. Rosynek, Isotherms and energetics of carbon dioxide adsorption on γ-alumina at 100–300°C, J. Phys. Chem., 79 (1975) 1280–1284.

[26] R.J. Cvetanovic and Y. Amenomiya, Applications of a temperature-programmed desorption technique to catalyst studies, Adv. Catal., 17 (1967) 103–149.